Possible doping strategies for MoS₂ monolayers: An *ab initio* study

Kapildeb Dolui, Ivan Rungger, Chaitanya Das Pemmaraju, and Stefano Sanvito

School of Physics and CRANN, Trinity College, Dublin 2, Ireland

Density functional theory is used to systematically study the electronic properties of doped MoS₂ monolayers, where the dopants are incorporated both via S/Mo substitution or as adsorbates. Among the possible substitutional dopants at the Mo site, Nb is identified as suitable *p*-type dopant, while Re is the donor with the lowest activation energy. When dopants are simply adsorbed on a monolayer we find that alkali metals shift the Fermi energy into the MoS₂ conduction band, making the system *n* type. Finally, the adsorption of charged molecules is considered, mimicking an ionic liquid environment. We find that molecules adsorption can lead to both *n*- and *p*-type conductivity, depending on the charge polarity of the adsorbed species.

I. INTRODUCTION

In recent years two dimensional (2D) materials have attracted a growing interest due to their potential for future nanoelectronics applications, owing to their unusual physical, optical, and electrical properties arising from the quantum confinement associated to their ultrathin structure.[1] These considerations apply particularly well to layered transition metal dichalcogenides (LTMDs) in which a multitude of electronic states have been observed, namely metallicity, semiconductivity, and charge density waves. Given the richness in the electronic properties it is not a surprise that this materials class has been called out as the ideal platform for a multitude of applications.[2,3] For example, the prototypical LTMD, molybdenum disulfide MoS₂, has been widely explored as lubricant[4], catalyst[5] and as lithium ion battery anode.[6]

Structurally MoS₂ consists of covalently bonded S-Mo-S 2D hexagonal planes (monolayers), which in the bulk are bound together in a layered structure by weak van der Waals forces.[7] Interestingly, the electronic properties of bulk MoS₂ show a strong dependence on the layer thickness.[8] Single MoS₂ monolayers are particularly intriguing. These display a direct band gap of 1.9 eV, which makes them a semiconducting alternative to gapless graphene. Indeed the band gap of graphene can be opened by fabricating nanoribbons[9] or by depositing it over a suitable substrate.[10] However, this comes at the cost of deteriorating the carrier mobility due to edge and impurity scattering.[11] In contrast, the absence of dangling bonds, the high crystallinity, and the low dimensionality make the performance of LTMDs comparable to those of currently existing Si transistors at the scaling limit.[12–14] MoS₂ monolayer based transistors have been recently demonstrated to operate at room temperature, with a mobility of at least 200 cm²/V s and on/off current ratios of 10^8 with low standby power dissipation.[15] Interestingly, both *n*-type[15–18] and *p*-type[19,20] conductivities have been reported for ultrathin MoS₂ layers, depending on the experimental details. The origin of such diverse conducting properties remains to date far from being clear.

The possible creation of Mo and/or S vacancies in MoS₂ monolayers during the growth cannot be used as a doping strategy, since those vacancies always produce deep trap states in the MoS₂ monolayer band gap.[21] In a recent study we have investigated how unintentional doping of the substrate holding a MoS₂ monolayer may determine its conductivity.[22] Here we explore possible strategies for doping directly into the MoS₂ monolayer. Although there are studies available on specific dopants for single layer MoS₂,[21,23–25] to our knowledge there is not yet a systematic investigation comparing the doping properties of the various defects, when they are incorporated in either a substitutional position or they are adsorbed on the surface. Moreover, it has been reported that in a liquid-gated electric double layer transistor, the ions can modulate the electronic properties from insulating to metallic through electrostatic induced carrier doping in the transport channel at a finite gate bias.[26] Compared with other dopants, such as metals and light atoms, ionic liquids have several advantages as surface dopants: a large variety of such ionic complexes are available, they can accumulate more carriers than conventional solid state gated transistors, and they do not induce structural disorder like substitutional dopants. In fact, ambipolar transistor operation has been achieved using thin flakes of MoS₂ in an ionic liquid gated environment.[27] The present work explores also this possibility.

Here we systematically study the effects of dopants on the electronic structure of a MoS₂ monolayer, by calculating the formation energies and the electronic properties of halogens, nonmetals, transition metals, and alkali metals added in various geometrical configurations. Our aim is that of identifying potential candidates for making MoS₂ monolayers either *n* or *p* type in a controlled way. Then we present an investigation of the electronic structure of MoS₂ monolayers when two molecular ions, NH_4^+ and BF_4^-, are adsorbed at the surface. The paper is organized as follows. After a brief discussion of the computational methods used we turn our attention to the case of substitutional doping by looking at both the S and the Mo site. Next we consider the case of doping by adsorption of alkali and molecular ions. At the end of the results section we briefly discuss the robustness of our calculations against the particular choice of exchange and correlation functional and finally we conclude.

II. METHODOLOGY

In order to investigate the electronic properties of a MoS₂ monolayer doped with impurities, *ab initio* calculations are performed using density functional theory[28,29] within the local
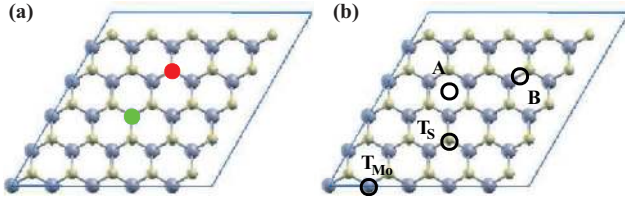
FIG. 1. (Color online) Structure of the supercell used for the calculations. In (a) we show a 5×5 MoS$_2$ monolayer supercell with the possible substitutional dopants. Mo is substituted by a transition metal (green dot): Y, Zr, Nb, Re, Rh, Ru, Pd, Ag, Cd; S is substituted by nonmetals and halogens (red dot): P, N, As; F, Cl, Br, I. In (b) we display the same supercell where we indicate the possible adsorption sites defined in the text. Light gray spheres indicate Mo atoms; light yellow spheres indicate S.

spin density approximation (DFT-LSDA) for the exchange and correlation potential. In particular we consider the Ceperley-Alder LSDA parametrization[30] as implemented in the SIESTA code.[31] In our calculations double-ζ polarized[32] numerical atomic orbitals basis sets are used for all atoms, and the Troullier-Martins scheme is used for constructing norm-conserving pseudopotentials.[33] A 5×5 hexagonal supercell [see Fig. 1(a)] with (15.66×15.66) Å^2 lateral dimensions is constructed and doping is introduced by replacing/adding a single atom in the supercell. This corresponds to simulating a Mo$_{1-x}$A$_x$S$_{2-y}$B$_y$ periodic system with $x = 4\%$ ($y = 2\%$) when the doping is at the Mo (S) site. An equivalent plane wave cutoff of 250 Ry is used for the real space mesh and the Brillouin zone is sampled over a $5 \times 5 \times 1$ Monkhorst-Pack k grid. Periodic boundary conditions are applied and a vacuum layer of at least 15 Å is placed above the monolayer to minimize the interaction between the adjacent periodic images. A temperature of 300 K is used when populating the electronic states with a Fermi distribution. The relaxed geometries are obtained by conjugate gradient, where all the atoms in the supercell are allowed to relax until any force is smaller than 0.02 eV/Å.

In order to verify that the calculated impurity level alignments are robust against the choice of exchange correlation functional, we repeat the calculations for the main results by using the screened hybrid functional of Heyd-Scuseria-Ernzerhof (HSE06).[34] All DFT calculations based on the HSE06 functional are carried out with the projector augmented wave (PAW) pseudopotential plane-wave method[35] as implemented in the VASP code.[36] A $3 \times 3 \times 1$ Monkhorst-Pack[37] k-point grid is employed and the plane wave energy cutoff is 500 eV.

The formation energy of a particular substitutional dopant, E_{form}, is defined as

$$E_{\text{form}} = E_{\text{tot}}[\text{MoS}_2^* + \text{X}] - E_{\text{tot}}[\text{MoS}_2] + \mu_{\text{host}} - \mu_{\text{X}}, \quad (1)$$

where $E_{\text{tot}}[\text{MoS}_2^* + \text{X}]$ is the total energy of the system including the substitutional atom X, $E_{\text{tot}}[\text{MoS}_2]$ is the total energy of the corresponding pristine MoS$_2$ monolayer, while μ_{X} and μ_{host} are respectively the chemical potentials of the substitutional atom X and of the substituted Mo (S) host atom. The chemical potentials of the X dopants are calculated with respect to bulk (X$_2$ dimers) reference levels for Mo (S) substitution. The formation energy of MoS$_2$ itself,

$E_{\text{form}}[\text{MoS}_2]$, can be calculated from the expression

$$E_{\text{form}}[\text{MoS}_2] = \mu_{\text{MoS}_2} - \mu_{\text{Mo}}^0 - 2\mu_{\text{S}}^0, \quad (2)$$

where μ_{MoS_2} is equal to $E_{\text{tot}}[\text{MoS}_2]$ per MoS$_2$ formula unit, and μ_{Mo}^0 (μ_{S}^0) is the total energy per atom of Mo (S) in its reference phase. For Mo the reference phase used is the bulk metallic body-centered-cubic (bcc) structure, whereas for S it is the S$_2$ molecule (we note that the choice of reference phase is not unique). The value of $E_{\text{form}}[\text{MoS}_2]$ is then calculated to -6.11 eV in DFT-LDA.

The value of μ_{host} in Eq. (1), and therefore also E_{form}, largely depends on the experimental growth conditions. As limiting cases we consider the Mo-rich and the S-rich situation. Under Mo-rich conditions the Mo chemical potential is equal to the bulk Mo value, $\mu_{\text{Mo}}^{\text{Mo-rich}} = \mu_{\text{Mo}}^0$. In thermodynamic equilibrium one can assume that $\mu_{\text{MoS2}} = \mu_{\text{Mo}} + 2\mu_{\text{S}}$, so that for Mo-rich conditions the S chemical potential is $\mu_{\text{S}}^{\text{Mo-rich}} = \frac{1}{2}(\mu_{\text{MoS2}} - \mu_{\text{Mo}}^0)$. Hence, by using Eq. (2), the chemical potentials for the Mo-rich limit can then be written as

$$\mu_{\text{Mo}}^{\text{Mo-rich}} = \mu_{\text{Mo}}^0, \quad (3)$$
$$\mu_{\text{S}}^{\text{Mo-rich}} = \mu_{\text{S}}^0 + \tfrac{1}{2}E_{\text{form}}[\text{MoS}_2]. \quad (4)$$

Analogously, for S-rich conditions one obtains

$$\mu_{\text{Mo}}^{\text{S-rich}} = \mu_{\text{Mo}}^0 + E_{\text{form}}[\text{MoS}_2], \quad (5)$$
$$\mu_{\text{S}}^{\text{S-rich}} = \mu_{\text{S}}^0. \quad (6)$$

In contrast the formation energy for an adsorbate, E_{ads}, can be written as

$$E_{\text{ads}} = E_{\text{tot}}[\text{MoS}_2 + \text{Y}] - E_{\text{tot}}[\text{MoS}_2] - E_{\text{bulk}}[\text{Y}], \quad (7)$$

where $E_{\text{tot}}[\text{MoS}_2 + \text{Y}]$ refers to the total energy when the adsorbate Y is attached to MoS$_2$, and $E_{\text{bulk}}[\text{Y}]$ is the energy of an adsorbate Y in its bulk form. In order to find the most stable configuration for adsorption, we consider four possible positions labeled as follows: T$_{\text{S}}$ (adsorbate on top of S), T$_{\text{Mo}}$ (adsorbate on top of Mo), A (adsorbate above the center of the hexagonal ring of MoS$_2$), and B (adsorbate above the middle of the Mo-S bond) [see Fig. 1(b)].

III. RESULTS AND DISCUSSION

Before discussing the formation energy and the electronic structure of the possible dopants let us here briefly review the electronic properties of a single MoS$_2$ monolayer. As the MoS$_2$ thickness is decreased from bulk to a few layers, the valence band minimum shifts from halfway along Γ-K line towards K.[8] For a monolayer the band gap becomes direct at K (see Fig. 2), a transition which has been recently observed experimentally.[8] The computed LSDA band gap of 1.86 eV is in good agreement with the experimental optical band gap of 1.90 eV,[16] although such an agreement has to be considered fortuitous. In fact the absorption edge of an optical excitation measures the energy difference between the quasiparticle band gap and the exciton binding energy. In MoS$_2$ monolayers this latter is of the order of 1 eV, as confirmed recently by many-body calculations.[38] Thus one expects that the true quasiparticle spectrum has a band gap of approximately 2.9 eV, in good agreement with that computed with the GW scheme, either at the first order level[38] (2.82 eV) or self-consistently[39] (2.76 eV). Note that
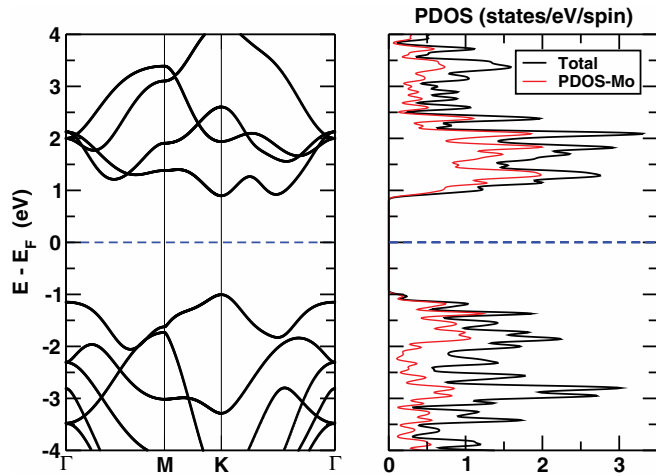
FIG. 2. (Color online) Band structure (left) and DOS (right) of a pristine (undoped) MoS$_2$ monolayer. The red curve indicates the DOS projected on the Mo atoms.

FIG. 3. (Color online) DOSs for a 5×5 MoS$_2$ supercell in which one S atom is replaced by (a) F, (b) Cl, (c) Br, and (d) I. Negative DOS values refer to minority spins, while positive are for the majority. The blue dashed line indicates the Fermi energy, while the colored shaded areas indicate the DOS projected over the dopants. Note that all the DOSs are aligned to have a common Fermi level, $E_F = 0$.

recently it has been reported for MoS$_2$[40] and BN[41] that, when periodic boundary conditions are applied, the value of the GW quasiparticle gap is sensitive to the amount of vacuum used in the calculations, and consequently extrapolation of the results to an infinite amount of vacuum is required to obtain converged results. It was found that the enhancement of the GW quasiparticle gap with the vacuum volume is compensated by the increase of the exciton binding energy, in such a way that the optical gap remains approximately constant. It has been shown that in the infinite vacuum limit (monolayer) the GW quasiparticle gap and the exciton binding energy converge to 2.97 eV and 1.1 eV, respectively, so that the resulting optical gap is 1.87 eV.[40] At the end of this section we will discuss how band-gap corrections, via the HSE06 functional, affect our main results. In any case, for both bulk and monolayer the band structure around the band gap is derived mainly from Mo $4d$ orbitals (see the orbital projected density of state, PDOS, in Fig. 2), although there are also small contributions in the valence band from the S $3p$ ones.

A. Substitutional doping

1. Substitution at the S site

We begin our analysis by substituting a surface S atom with elements taken from the halogen family, namely F, Cl, Br, and I. These are expected to act as a source of n-type doping for MoS$_2$, since they have one additional p electron with respect to S. The DOSs for the supercell including one atom of the halogen family are presented in Fig. 3. As a representative system, we discuss in detail results for Cl doping, since the other halogens present a similar electronic structure. A Cl-doped MoS$_2$ monolayer has a magnetic ground state, where an occupied defect level is formed at about 0.4 eV below the conduction band minimum (CBM). The corresponding minority state is located above the CBM and is empty. These defect levels originate from the hybridization between the Cl $3p$ and the Mo $4d$ states. Similar to the Cl substitution, for both F and Br dopants (isoelectronic to Cl) the system is paramagnetic, having a magnetic moment of
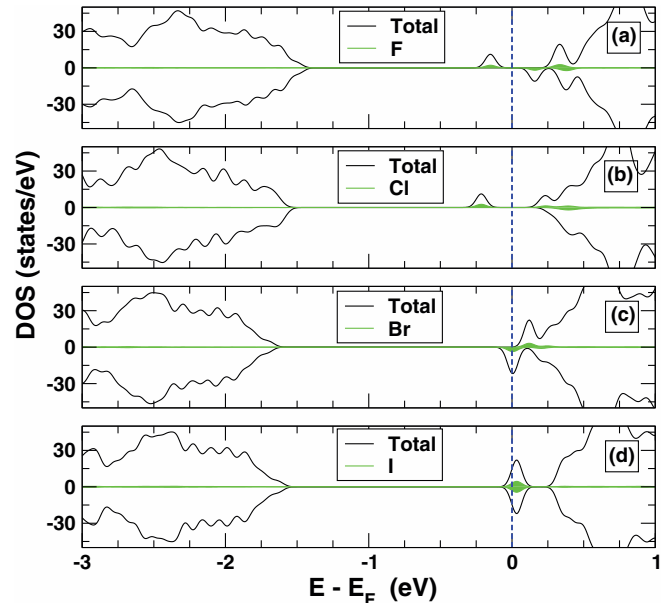
approximately 1 μ_B. In the case of F substituting S, the spin splitting is larger than that of Cl, whereas it is smaller for the Br substitutional case. Eventually, when S is replaced by iodine, the impurity becomes nonmagnetic, although the impurity level is still located well below (0.3 eV) the CBM [see Fig. 3(d)]. Note that having an impurity presenting a ground state with finite magnetic moment has nothing to do with diluted ferromagnetism in p-type systems, as sometimes erroneously claimed in literature. This simply indicates that the additional electron remains unpaired and localized around the impurity.[42] The dependence of the spin splitting of the impurity level on the atomic number simply follows the well-known trend for the exchange-correlation integral.[43]

We then investigate the possibility of p-type doping obtained by replacing an S atom with a group V element of the Periodic Table, namely N, P, and As (see Fig. 4). In the case of N the supercell has a magnetic ground state [see Fig. 4(a)], with a magnetic moment of 1 μ_B and a spin splitting of about 0.20 eV. In both the spin channels gap states are introduced above the valence band maximum (VBM), and these are formed by hybridization between the N $2p$ and the Mo $4d$ valence orbitals. Similarly, when substituting S with P, the system is again magnetic, but the defect states are rigidly shifted closer to the VBM of the pristine MoS$_2$ monolayer in both the spin channels. The spin splitting remains similar to that of N. Finally, for the As substitutional case, the defect states shift even more towards the VBM. Additionally, the spin splitting vanishes and the system becomes a p-type semiconductor. The partially unoccupied impurity band however shows very little dispersion and it is separated from the valence band by about 0.08 eV. Such an impurity band is formed mainly by As $4p$ and Mo $4d$ orbitals.
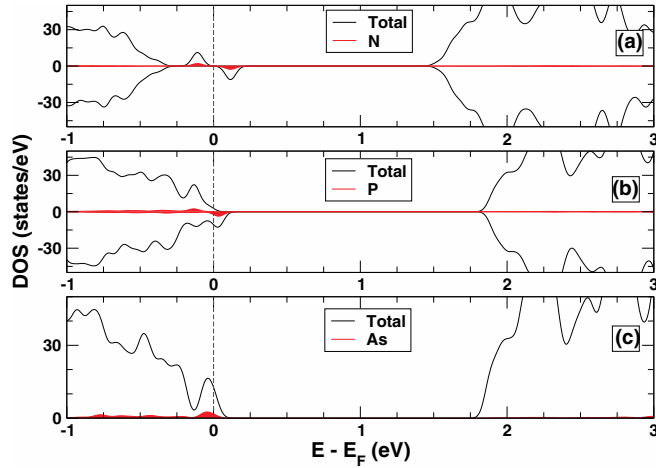
FIG. 4. (Color online) DOSs for a 5×5 MoS$_2$ supercell in which one S atom is replaced by (a) N, (b) P, and (c) As. Negative values refer to minority spins and positive values to majority spins. The blue dashed line indicates the Fermi energy; the colored shaded areas indicate the DOS projected on the dopants. Note that all the DOSs are aligned to have a common Fermi level, $E_F = 0$.

To summarize our results for S substituting impurities, we find that most dopants create localized, spin-polarized, gap states. When increasing the dopant atomic number the spin-splitting reduces and the states move towards the VBM/CBM. Among the many dopants investigated, As appears to give the most promising DOS for p-type doping, since the associated diamagnetic impurity band is very close to the VBM. In the case of n-type doping, all substituent dopants have donor states located rather far from the MoS$_2$ CBM and therefore they are rather localized. In addition to these considerations a look at Table I, where we present the formation energy of the various dopants, reveals that all the S substituents possess a rather large positive formation energy under the S-rich limit, i.e.,

TABLE I. Theoretically calculated magnetic moment, m, and the formation energy, E_{form}, of different substitutional dopants in the MoS$_2$ monolayer for Mo-rich and for S-rich conditions.

Impurity	m (μ_B/impurity)	E_{form} (eV)	
		S-rich	Mo-rich
F	1.00	0.60	−2.45
Cl	1.00	1.93	−1.12
Br	1.00	2.16	−0.89
I	0.00	2.53	−0.52
N	1.00	2.90	−0.15
P	1.00	1.89	−1.16
As	0.00	1.91	−1.14
Re	1.00	−4.06	2.05
Ru	2.00	−3.06	3.05
Rh	3.00	−1.96	4.15
Pd	4.00	−0.48	5.63
Ag	2.57	1.17	7.28
Cd	1.58	−0.01	6.10
Nb	0.00	−6.29	−0.19
Zr	0.00	−6.59	−0.48
Y	0.00	−5.59	0.52

they are unlikely to form under equilibrium thermodynamical conditions. The only viable formation channel is offered by filling S vacancies, which have been recently demonstrated to form with relative ease.[44] Therefore, it appears that a strategy for doping at the S site may be that of growing S poor samples and then of filling the vacancies with an appropriate donor/acceptor sulfur replacement. Indeed the formation energies are negative in the Mo-rich (equivalent to S-poor) limit both for the p- and n-type dopants (Table I). This reflects the fact that the formation energy is largely dependent on the growth conditions. The large variation of the formation energies for S substitutions in a MoS$_2$ monolayer with respect to different values of μ_S has been reported also in Ref. 44.

2. Substitution at the Mo site

Next we consider substitutional doping at the Mo site with different transition metal atoms having a growing number of electrons in the d shell. Specifically we consider all the $4d$ elements in the Periodic Table ranging from Y to Cd with the only exception of radioactive Tc, which is replaced by Re ($5d$). In general we find that for all the substitutional atoms having a d occupancy larger than Mo, the ground state is spin polarized, while Y, Zr, and Nb have a diamagnetic ground state (see Table I).

Let us again discuss the case of n-type doping first. When Re replaces Mo, one extra electron is added to the supercell. This remains unpaired and occupies a majority spins gap state [Fig. 5(a)], located 0.3 eV below the CBM, with the Fermi energy, E_F, located between such state and the CBM. As a consequence the supercell has a magnetic moment of $1 \mu_B$ and the DOS for this situation resembles that of Cl substituting S [Fig. 3(b)]. If one forces a non-spin-polarized solution for Re-doped MoS$_2$ monolayer, the donor level is created at about 0.2 eV below the CBM. However, the magnetic ground state is lower in energy than the nonmagnetic one by 82 meV/supercell, i.e., a diamagnetic solution is not stable. Note that our non-spin-polarized result is consistent to that reported for a similar calculation,[45] where a Re donor level at 0.19 eV below the CBM suggested that Re could be used as n-type dopant in MoS$_2$ nanotubes. Such a result thus seems to be robust against spin polarization (the spin polarized impurity state is at 0.3 eV below the VBM). Note that single crystals Re-doped MoS$_2$ have been grown in the past by chemical vapor deposition.[46]

When one then looks at other transition metal dopants having a d-orbitals occupancy larger than Re, an increasing number of gap states is formed. These are progressively occupied so that the excess electrons do not spill into the MoS$_2$ conduction band (see Fig. 5). As a consequence the Fermi energy always lies in the MoS$_2$ band gap, and in fact it moves deeper into the band gap as the d shell filling of the dopant increases. The excess electrons first fill up the majority spin states of the host d orbitals, until the magnetic moment of the impurity reaches the largest value of $4 \mu_B$ for Pd. Then the magnetic moment decreases for Ag and Cd as the additional electrons start to populate the minority spins states (see Table I).

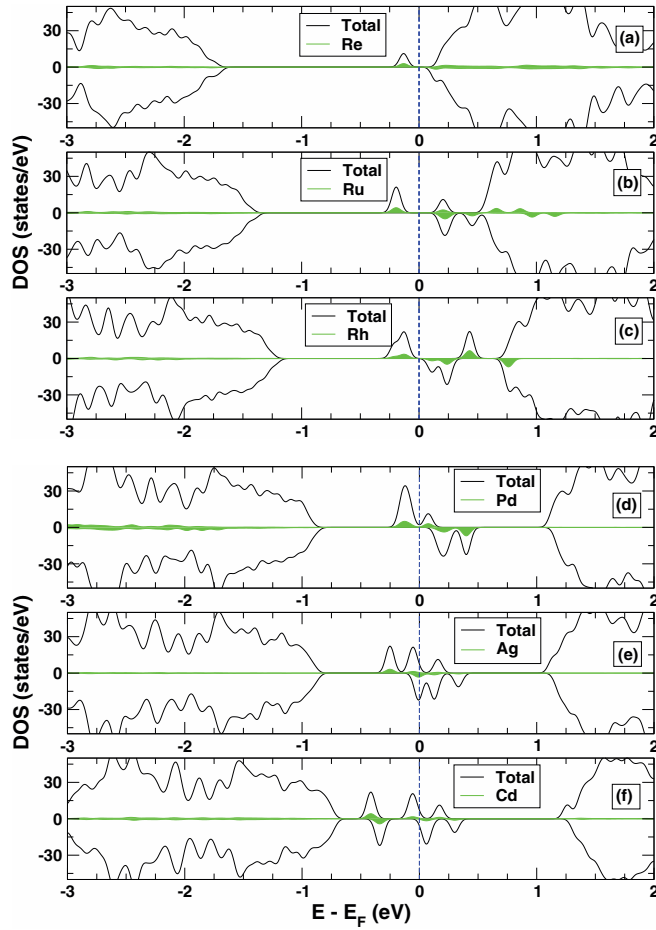Next we move to study the possibility of obtaining p-type doping by replacing Mo with Nb, Zr, and Y, which have

FIG. 5. (Color online) DOSs for a 5×5 MoS$_2$ supercell in which one Mo atom is replaced by (a) Re, (b) Ru, (c) Rh, (d) Pd, (e) Ag, and (f) Cd. The blue dashed line marks the Fermi energy; the colored shaded areas indicate the DOS projected onto the dopants. Note that all the DOSs are aligned to have a common Fermi level, $E_F = 0$.

FIG. 6. (Color online) DOSs for a 5×5 MoS$_2$ supercell in which one Mo atom is replaced by (a) Nb, (b) Zr, and (c) Y. The blue dashed line indicates the Fermi energy, the colored shaded areas indicate the DOS projected on the dopants. Note that all the DOSs are aligned to have a common Fermi level, $E_F = 0$.

respectively one, two, and three electrons less than Mo. The case of Nb seems to be particularly attractive. The inclusion of Nb into MoS$_2$ changes little the bond lengths and also the main DOS. The only notable effect is the shift of the Fermi energy below the VBM due to the one electron removal [see Fig. 6(a)]. The newly created defect states are rather delocalized and the charge excess spreads out up to the third nearest neighbor Mo atoms. The states around the VBM mainly originate from hybridized d orbitals of Nb and Mo. The valence band now looks sufficiently dispersive in our DFT band structure, and therefore the mobility is expected to be rather large. Importantly, under Mo-rich conditions the formation energy for Nb doping is -0.19 eV, in good agreement with the formation energy of -0.21 eV[47] obtained theoretically for Nb doping in bulk MoS$_2$. The formation energy is even more negative in the S-rich limit, suggesting that the S-rich limit is more favorable for Nb substitution compared to the Mo-rich one. Overall, our results suggest that Nb may be a promising candidate as p-type dopant in MoS$_2$ monolayers. Note that an experimental study[48] shows that Nb-substituted (concentration range 15%–25%) MoS$_2$ nanoparticles can be synthesized, and that they also exhibit p-type character. Finally, for all the other two p-type dopants considered (Y and Zr) the ground state
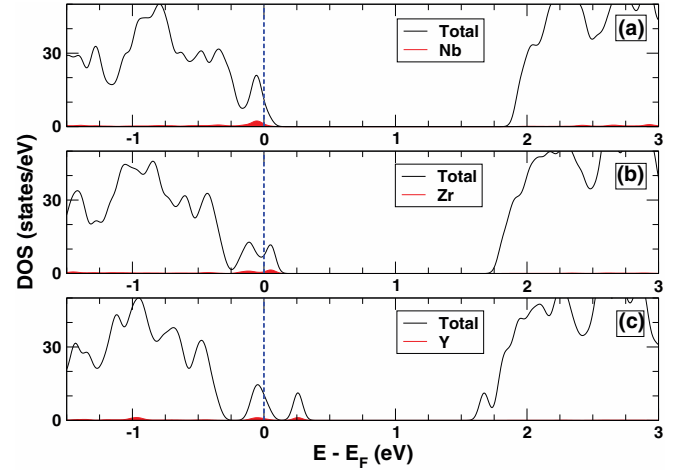
is also nonmagnetic (see Table I). However, in contrast to Nb doping, the defect state becomes less hybridized with the VBM and produces split off acceptor levels above the VBM for both Zr and Y [see Figs. 6(b) and 6(c)].

We conclude this section by evaluating the pairing energy between two Nb atoms placed in a 6×6 supercell. In Table II we list the energy difference δE between the configuration where the two impurities are placed at nearest neighbor positions and when they are placed as far as possible in the supercell. The result suggests that in the case of Nb pairs the dopants tend to stay close to each other in the MoS$_2$ monolayer ($\delta E < 0$). Thus, based solely on the pairing energy, Nb dopants would form clusters. Clustering however is likely to be inhibited by the large energy barrier for Nb diffusion in the MoS$_2$ plane.

Summarizing the situation for transition metal doping at the Mo site we find that, when the dopant has more d electrons than Mo, donor states are created deep inside the MoS$_2$ band gap (at least 0.2 eV below the CBM), with Re being the dopant with the smallest activation energy. Similar to the results for S substitution, in all cases the formation energies are largely dependent on the growth conditions: while they are positive in the Mo-rich limit, with the exception of Ag they all become negative under S-rich conditions (Table I). On the contrary, p-type doping obtained by substituting Mo with transition metals such as Nb and Zr creates acceptor states just at the VBM, and the formation energies are also small (Table I). In fact, for both

TABLE II. Pairing energy for two impurities doping a MoS$_2$ monolayer. Calculations are based on total energy difference between a nearest neighbor and a separated geometry in a 6×6 supercell. Negative δE indicate a tendency to clustering.

Atom-Atom	δE (meV)
Nb-Nb	-157
Cs-Cs	166
Nb-Cs	-218

Nb and Zr, E_{form} is negative, indicating that substitutional doping will form spontaneously in MoS_2 monolayers (note that this is relative to the bulk reference for the dopant). In contrast, the formation energies for Nb, Zr, and Y have large negative values in the S-rich limit. Intriguingly, also for the case of transition metal doping at the Mo site the possibility of filling vacancies remains open. In fact a recent experiment[49] has provided evidence for the formation of Mo vacancies in bulk MoS_2 via proton irradiation.

B. Doping by adsorption

The results of the previous section show that neither Mo substitution with transition metals nor S substitution with nonmetal elements appear as promising strategies for obtaining shallow donor states (p doping is much more promising with Nb). Another possible route for obtaining n-type MoS_2 monolayers is by adsorbing H or alkali metals such as Li, K, and Cs. This possibility is explored here. Then, in the second part of this section we consider adsorbed molecular ions as potential dopants with both n- and p-type character.

1. Alkali atom adsorption

Among all the possible adsorption sites for alkali metals on the MoS_2 surface, we find that the T_{Mo} one [see Fig. 1(b)] is the most energetically favorable. This is also suggested experimentally,[50] as well as predicted by previous theoretical calculations.[51] Most importantly all the adsorption energies are found large and negative (see Table III) indicating thermodynamical stability.

We start by considering Cs adsorption. When Cs is adsorbed on a MoS_2 monolayer there is no significant change in the geometry, i.e., the ion binds without distorting the lattice of the host. The DOS presented in Fig. 7(a) shows that the available Cs $6s$ electron is transferred to the CBM of the MoS_2 monolayer, occupying the Mo $4d$ orbitals. In this case there is no split off at the bottom of the conduction band and the DOS projected over the Cs $6s$ orbitals appears uniformly spread over a 1.5 eV energy window. This essentially means that Cs adsorbed over a MoS_2 monolayer acts as the perfect donor. A very similar situation is found for both K and Li, with only minor quantitative differences in the spread of the DOS associated with the s shell of the dopant [see Fig. 7(b) and Fig. 7(c)]. In contrast, the adsorption of H produces a spin-split state 1 eV below the CBM, i.e., roughly at midgap of the LSDA band gap (see Fig. 7). As such we conclude that H is not a shallow donor for MoS_2, in good agreement with the recent theoretical results.[44] The stability of the doped systems depends on the energy barrier for migration of the adsorbed atoms on the MoS_2 surface. We evaluate the minimum energy pathway and the resulting energy barrier between two adjacent
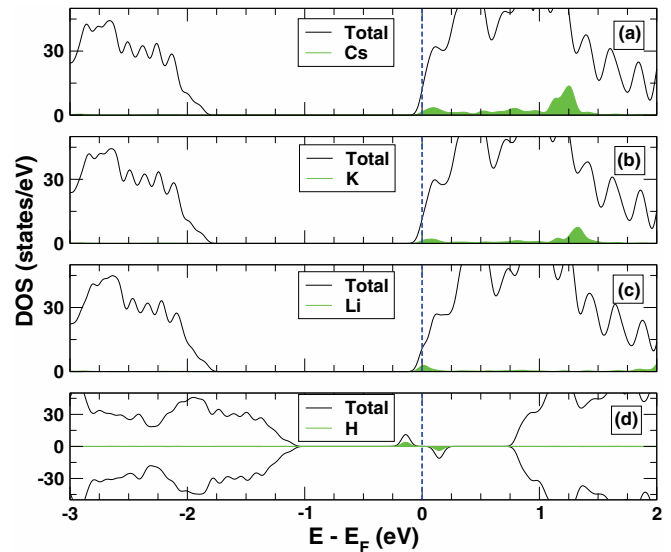
TABLE III. Theoretically calculated adsorption energy for different alkali metal adsorbed on the MoS_2 monolayer.

Adatom	E_{ads} (eV)
Cs	−0.79
K	−0.82
Li	−0.98

FIG. 7. (Color online) DOSs for a 5×5 MoS_2 supercell in which an atom chosen between (a) Cs, (b) K, (c) Li, and (d) H is adsorbed on the MoS_2 surface. The blue dashed line indicates the Fermi energy; the colored shaded areas indicate the DOS projected on the adsorbates. Note that all the DOSs are aligned to have a common Fermi level, $E_F = 0$.

binding sites using the nudged elastic band (NEB) method implemented in SIESTA.[52]

Next we calculate the migration barrier for adatom adsorbed on the MoS_2 surfaces. The bisection-image nudged elastic band (bisection-NEB) method implemented in SIESTA[52] was used to determine the energy barrier and the minimum energy pathways. The calculated values for the migration barriers are 0.1, 0.15, 0.24, and 0.26 eV for Cs, K, Li, and H, respectively. For such barriers migration of the adatoms at room temperature is possible, especially for the heavier adatoms, which is detrimental for the stability of the system. Note, however, that in a device the MoS_2 surface will usually be covered by a capping layer, which will increase these energy barriers, so that it is possible that the migration of the dopants is suppressed.

The pairing energies between two Cs atoms and between Nb and Cs are given in Table II. Our total energy calculations suggest that pairing between Cs atoms is not energetically favorable. On the other hand, Cs atoms can reduce their energy if they are adsorbed close to a Nb atom rather than on the top of a Mo atom. This can be easily explained with the electrostatic attraction between the two oppositely charged defects. This case of codoping with Cs and Nb is particularly interesting, since it can be used as a strategy for fabricating p-n junctions, or more generally devices that require both n-type and p-type conductivity. Importantly, the DOS of a supercell where a Mo-substitutional Nb impurity is bonded to a Cs adatom appears essentially identical to that of an undoped MoS_2 monolayer (see Fig. 8), indicating that charge compensation is very effective. As a consequence our results suggest that an effective strategy for creating p-n heterojunctions must prevent the formation of Cs-Nb bonding by suppressing the migration of Cs on the surface.

In summary, we find that adsorbed alkali metals release their valance s electron to the MoS_2 conduction band, and
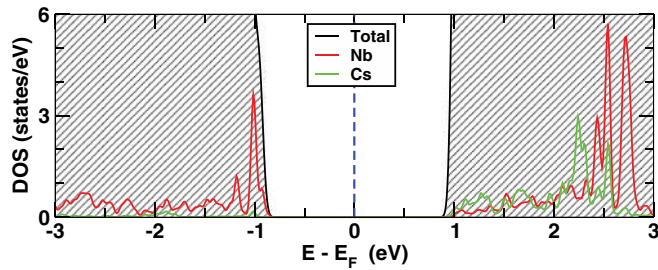
FIG. 8. (Color online) DOS for a MoS$_2$ supercell, where a single Mo is replaced by Nb, and where a Cs atom is adsorbed. The blue dashed line indicates the Fermi energy, $E_F = 0$; the colored curves indicate the DOS projected on the dopants.

that the adsorption energies are large and negative, meaning that the doping will occur easily. Therefore, adsorbed alkali metals, with the exception of H, appear as ideal candidates for doping n-type MoS$_2$. To put this result in context we remark that various experimental studies have demonstrated the possibility of dope n-type bulk MoS$_2$ by intercalating alkali metals.[3] Here we demonstrate that the same is also possible at the single layer level.

2. Adsorption of molecular ions

Electric double layer (EDL) transistors with ionic liquids (ILs) employed as gate dielectrics have recently emerged as promising devices, where the electrical properties of a solid can be controlled by electrostatic carrier doping.[26,53] A schematic diagram for such a device is shown in Fig. 9. By applying a gate bias to the ionic liquid, an electric double layer is formed between the interface of the liquid and the solid (see Fig. 9). Here the polarity of the molecular ions on the surface of
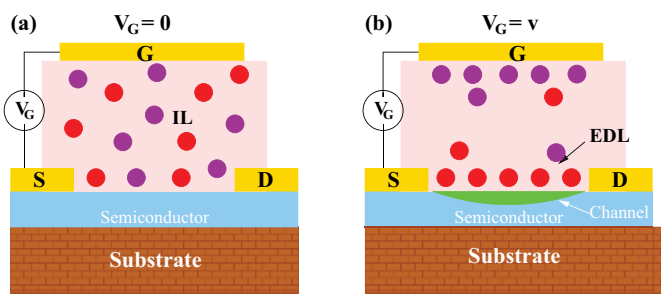

FIG. 9. (Color online) Schematic diagrams of the electric double layer transistor operation with an ionic liquid electrolyte. Here, "S" indicates the source, "D" indicates the drain, and "G" indicates the gate. The solid circles denote the ions in the liquid, where the different colors represent cations and anions. (a) When no gate voltage is applied ($V_G = 0$), cations and anions are uniformly distributed and both adsorbed at the interface of the semiconductor with equal probability. (b) When a finite gate bias is present ($V_G = v$), cations or anions adsorb predominantly at the gate electrode, depending on the bias polarity, and the oppositely charged ions adsorb predominantly on the semiconductor. These adsorbed ions lead to an accumulation of a screening charge at the semiconductor surface, which implies a large surface carrier concentration.
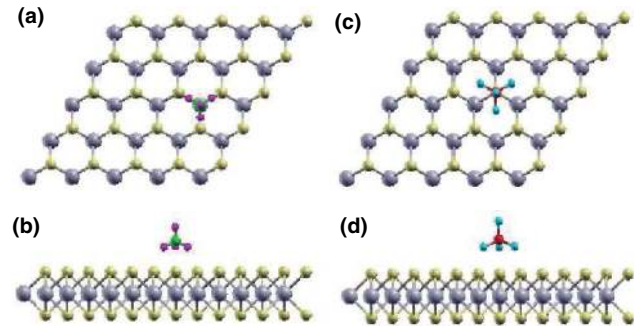

FIG. 10. (Color online) Optimized geometries for [(a),(b)] NH$_4^+$ and [(c),(d)] BF$_4^-$ ions adsorbed on a MoS$_2$ monolayer. In (a) and (c) the top view is shown, whereas the side view is in (b) and (d). Pink spheres indicate H, green spheres N, cyan spheres F, and red spheres B.

the semiconductor can be reversed by changing the polarity of the gate bias. The accumulation of high charge carrier densities is possible ($\sim 10^{14}$ cm^{-2}) and this can be modulated by the applied gate voltage. In some cases, the accumulation can be so large as to lead to phase transitions in the solid. Metal-superconductor and metal-insulator transitions have been demonstrated in KTiO$_3$[54] and VO$_2$,[26] respectively. The operation of highly flexible MoS$_2$ thin-film transistors in an ionic liquid gated dielectric has been demonstrated recently.[55] Here we discuss the effects of the adsorbed molecular ions on the MoS$_2$ monolayer.

A variety of different ionic liquids are experimentally available. Here we consider NH$_4^+$ as cation and BF$_4^-$ as anion, and we place them on the 5×5 MoS$_2$ supercell (see Fig. 10). Such geometry corresponds to an impurity density of $\sim 10^{14}$ cm^{-2}. Note that neutral molecules are used in our calculations. When adsorbing them on the MoS$_2$ surface they take (give) one electron from (to) the MoS$_2$ monolayer, so that at self-consistency the molecules and the MoS$_2$ substrate have opposite charge (overall the simulation cell is charge neutral). We find that the most energetically favorable adsorption site is T$_S$ for the cation and T$_{Mo}$ for the anion. In Fig. 11(a) the DOS is shown for NH$_4$ adsorption. It can be seen that the NH$_4$ releases one electron into the MoS$_2$ conduction band, resulting in a n-type MoS$_2$ monolayer channel. In contrast, when BF$_4$ is adsorbed, one electron is transferred from MoS$_2$ to the molecule [see Fig. 11(b)]. As a consequence the Fermi energy shifts below the MoS$_2$ VBM, so that the system becomes p type. This also confirms the fact that the adsorbed molecules are indeed ionized to NH$_4^+$ and BF$_4^-$ when put on MoS$_2$. In a liquid gated transistor arrangement, the anions/cations are brought close to the surface of the channel by applying a bias at the gate. Therefore, for this system, depending on the polarity of the gate bias the MoS$_2$ is indeed predicted to have a n- or p-type conducting channel. Clearly this effect is maximized for a single layer of MoS$_2$ when compared to thicker structures. In fact, conductivity measurements[27] on MoS$_2$ show that EDL gating becomes less efficient when going from a thin layer to bulk. Moreover, depending on the polarity of the bias, it is found that the conductivity indeed switches from n type to p type.
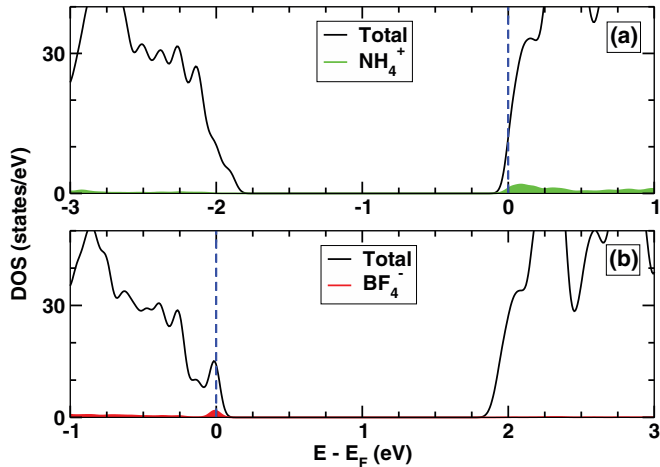
FIG. 11. (Color online) DOS for (a) NH_4^+ and (b) BF_4^- molecule adsorbed on MoS_2. The results reported here are for a 5×5 supercell. The blue dashed line indicates the Fermi energy; the colored shaded areas indicate the DOS projected over the adsorbates. Note that the DOSs have the Fermi level at 0 ($E_F = 0$), but they are aligned according to their valence and conduction bands.

C. Robustness of the results against the choice of XC functional: HSE06

Finally, in order to verify that the impurity level alignment presented in the previous sections is robust against the level of approximation taken for the DFT exchange-correlation energy, we here repeat our calculations by using the HSE06 functional. The MoS_2 lattice constant obtained with HSE06 is 3.155 Å, which is only slightly larger than the LSDA value of 3.137 Å. For a pristine MoS_2 monolayer at this relaxed lattice constant HSE06 exhibits a direct band gap of 2.2 eV (compared to a LDA band gap of 1.86 eV). This is rather similar to the band gap obtained by applying the atomic self-interaction correction scheme.[22]

In Fig. 12 we report our results for four representative doping strategies, namely for Nb substitutional doping, as well as for Cs, NH_4, and BF_4 adsorption. These correspond to the most promising dopants for either *n*-type or *p*-type doping as obtained at the LSDA level. The calculations are carried out with the same structures used in the previous sections, in order to make a direct comparison between results obtained with the two functionals used. We note, however, that the MoS_2 band gap is very sensitive to changes in the lattice constant,[56] so that the HSE06 band gap at the LSDA lattice constant of 3.137 Å becomes 2.31 eV. We find that for all the four cases the main difference between the LSDA and the HSE06 results is just a change in the band gap, while the impurity levels with respect to the relative Fermi energy are placed at the same position. Therefore, we can conclude that the four most promising candidates for doping MoS_2 monolayers remain those identified by our initial LSDA analysis. Note that for deeper donor and deep acceptor levels the differences between HSE and LDA might become more pronounced, since those states are more localized compared to shallow donor and acceptor levels, so that the self-interaction error in LDA is larger. It is expected that by using HSE, which corrects the self-interaction error, these states become even more localized
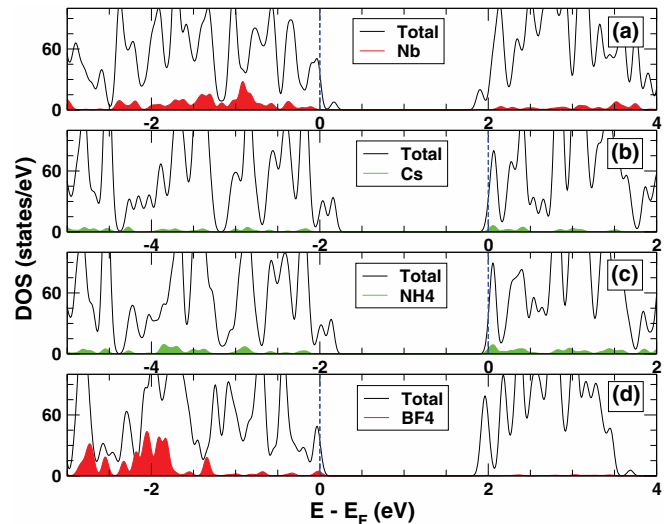

FIG. 12. (Color online) DOSs for the doped MoS_2 monolayer, calculated with the HSE06 functional. We report results for (a) Nb substitutional at the Mo site, and for (b) Cs, (c) NH_4^+, and (d) BF_4^- adsorbed on the MoS_2 surface. The blue dashed line indicates the Fermi energy ($E_F = 0$); the colored shaded areas indicate the DOS projected on the adsorbates. In the plot we have aligned all the conduction and valence bands.

than already predicted by LDA, further confirming that they are not optimal candidates for doping.

IV. CONCLUSION

We have carried out a systematic study on the changes to the electronic structure of a MoS_2 monolayer induced by various dopants. This study has the aim of identifying possible doping strategies for MoS_2 monolayers to be used in devices manufacturing. We have considered first substitutional doping at both the Mo and the S site, as well as doping by adsorption. In general, S substitution with nonmetals and Mo substitution with transition metals create deep donor levels inside the band gap of the MoS_2 monolayer for most of the dopants considered. However, with substitutional doping we find that it is possible to obtain *p*-type MoS_2 by replacing a Mo atom with Nb. In contrast *n*-type doping does not appear possible since we have found deep donor levels for all the substitutions investigated (either at the Mo or the S site). More promising *n*-type doping can be achieved by adsorbing alkali metals on the surface of MoS_2. Finally, as a last class of dopants, we have considered the adsorption of ionic molecules, which occurs during the electric double layer formation in MoS_2 embedded in an ionic liquid. These show high potential for inducing large carrier concentrations within the MoS_2 monolayer, in the form of both electrons or holes.

[1] A. H. Castro Neto and K. Novoselov, Rep. Prog. Phys. **74**, 082501 (2011).

[2] J. A. Wilson and A. D. Yoffe, Adv. Phys. **18**, 193 (1969).

[3] R. H. Friend and A. D. Yoffe, Adv. Phys. **36**, 1 (1987).

[4] W. O. Winer, Wear **10**, 422 (1967).

[5] H. Topsøe, B. Hinnemann, J. K. Nørskov, J. V. Lauritsen, F. Besenbacher, P. L. Hansen, G. Hytoft, R. G. Egeberg, and K. G. Knudsen, Catal. Today **107**, 12 (2005).

[6] X. Fang, X. Guo, Y. Mao, C. Hua, L. Shen, Y. Hu, Z. Wang, F. Wu, and L. Chen, Chem. Asian J. **7**, 1013 (2012).

[7] K. K. Tiong and T. S. Shou, J. Phys.: Condens. Matter **12**, 5043 (2000).

[8] A. Splendiani, L. Sun, Y. Zhang, T. Li, J. Kim, C.-Y. Chim, G. Galli, and F. Wang, Nano Lett. **10**, 1271 (2010).

[9] X. Wang, Y. Ouyang, X. Li, H. Wang, J. Guo, and H. Dai, Phys. Rev. Lett. **100**, 206803 (2008).

[10] S. Y. Zhou, G.-H. Gweon, A. V. Fedorov, P. N. First, W. A. de Heer, D.-H. Lee, F. Guinea, A. H. Castro Neto, and A. Lanzara, Nat. Mater. **6**, 770 (2007).

[11] S. Adam, E. H. Hwang, V. M. Galitski, and S. D. Sarma, Proc. Natl. Acad. Sci. USA **104**, 18392 (2007).

[12] A. Ayari, E. Cobas, O. Ogundadegbe, and M. S. Fuhrer, J. Appl. Phys. **101**, 014507 (2007).

[13] K.-K. Liu, W. Zhang, Y.-H. Lee, Y.-C. Lin, M.-T. Chang, C.-Y. Su, C.-S. Chang, H. Li, Y. Shi, H. Zhang, C.-S. Lai, and L.-J. Li, Nano Lett. **12**, 1538 (2012).

[14] L. Liu, S. B. Kumar, Y. Ouyang, and J. Guo, IEEE Trans. Electron. Dev. **58**, 3042 (2011).

[15] B. Radisavljevic, A. Radenovic, J. Brivio, V. Giacometti, and A. Kis, Nat. Nanotechnol. **6**, 147 (2011).

[16] K. F. Mak, C. Lee, J. Hone, J. Shan, and T. F. Heinz, Phys. Rev. Lett. **105**, 136805 (2010).

[17] H. Li, G. Lu, Z. Yin, Q. He, H. Li, Q. Zhang, and H. Zhan, Small **8**, 682 (2012).

[18] Y.-H. Lee, X.-Q. Zhang, W. Zhang, M.-T. Chang, C.-T. Lin, K.-D. Chang, Y.-C. Yu, J. Tse-Wei Wang, C.-S. Chang, L.-J. Li, and T.-W. Lin, Adv. Mater. **24**, 2320 (2012).

[19] Z. Zeng, Z. Yin, X. Huang, H. Li, Q. He, G. Lu, F. Boey, and H. Zhang, Angew. Chem., Int. Ed. **50**, 11093 (2011).

[20] Y. Zhan, Z. Liu, S. Najmaei, P. M. Ajayan, and J. Lou, Small **8**, 966 (2012).

[21] J. D. Fuhr, A. Saúl, and J. O. Sofo, Phys. Rev. Lett. **92**, 026802 (2004).

[22] K. Dolui, I. Rungger, and S. Sanvito, Phys. Rev. B **87**, 165402 (2013).

[23] J. He, K. Wu, R. Sa, Q. Li, and Y. Wei, Appl. Phys. Lett. **96**, 082504 (2010).

[24] Y. C. Cheng, Z. Y. Zhu, W. B. Mi, Z. B. Guo, and U. Schwingenschlögl, Phys. Rev. B **87**, 100401 (2013).

[25] C. Ataca and S. Ciraci, J. Phys. Chem. C **115**, 13303 (2011).

[26] H. Ji, J. Wei, and D. Natelson, Nano Lett. **12**, 2988 (2012).

[27] Y. Zhang, J. Ye, Y. Matsuhashi, and Y. Iwasa, Nano Lett. **12**, 1136 (2012).

[28] P. Hohenberg and W. Kohn, Phys. Rev. **136**, B864 (1964).

[29] W. Kohn and L. J. Sham, Phys. Rev. **140**, A1133 (1965).

[30] D. M. Ceperley and B. J. Alder, Phys. Rev. Lett. **45**, 566 (1980).

[31] J. M. Soler, E. Artacho, J. D. Gale, A. Gracía, J. Junquera, P. Ordejón, and D. Sánchez-Porta, J. Phys.: Condens. Matter **14**, 2745 (2002).

[32] J. Junquera, Ó. Paz, D. Sánchez-Portal, and E. Artacho, Phys. Rev. B **64**, 235111 (2001).

[33] N. Troullier and J. L. Martins, Phys. Rev. B **43**, 1993 (1991).

[34] J. Heyd, G. E. Scuseria, and M. Ernzerhof, J. Chem. Phys. **118**, 8207 (2003); **124**, 219906 (2006).

[35] P. E. Blöchl, Phys. Rev. B **50**, 17953 (1994).

[36] G. Kresse and J. Furthmüller, Phys. Rev. B **54**, 11169 (1996).

[37] H. J. Monkhorst and J. D. Pack, Phys. Rev. B **13**, 5188 (1976).

[38] A. Ramasubramaniam, Phys. Rev. B **86**, 115409 (2012).

[39] T. Cheiwchanchamnangij and W. R. L. Lambrecht, Phys. Rev. B **85**, 205302 (2012).

[40] H.-P. Komsa and A. V. Krasheninnikov, Phys. Rev. B **86**, 241201(R) (2012).

[41] L. Wirtz, A. Marini, and A. Rubio, Phys. Rev. Lett. **96**, 126104 (2006).

[42] A. Droghetti, C. D. Pemmaraju, and S. Sanvito, Phys. Rev. B **78**, 140404(R) (2008).

[43] J. F. Janak, Phys. Rev. B **16**, 255 (1977).

[44] H.-P. Komsa, J. Kotakoski, S. Kurasch, O. Lehtinen, U. Kaiser, and A. V. Krasheninnikov, Phys. Rev. Lett. **109**, 035503 (2012).

[45] F. L. Deepak, R. P. Biro, Y. Feldman, H. Cohen, A. Enyashin, G. Seifert, and R. Tenne, Chem. Asian J. **3**, 1568 (2008).

[46] K. K. Tiong, P. C. Liao, C. H. Ho, and Y. S. Huang, J. Cryst. Growth **205**, 543 (1999).

[47] V. V. Ivanovskaya, A. Zobelli, A. Gloter, N. Brun, V. Serin, and C. Colliex, Phys. Rev. B **78**, 134104 (2008).

[48] F. L. Deepak *et al.*, J. Am. Chem. Soc. **129**, 12549 (2007).

[49] S. Mathew, K. Gopinadhan, T. K. Chan, X. J. Yu, D. Zhan, L. Cao, A. Rusydi, M. B. H. Breese, S. Dhar, Z. X. Shen, T. Venkatesan, and J. T. L. Thong, Appl. Phys. Lett. **101**, 102103 (2012).

[50] K. T. Park, J. S. Hess, and K. Klier, J. Chem. Phys. **111**, 1636 (1999).

[51] K. T. Park and J. Kong, Top. Catal. **18**, 175 (2002).

[52] T. Ohto, I. Rungger, K. Yamashita, H. Nakamura, and S. Sanvito, Phys. Rev. B **87**, 205439 (2013).

[53] H. T. Yuan, M. Tih, K. Morimoto, W. Tan, F. Wei, H. Shimotani, Ch. Kloc, and Y. Iwasa, Appl. Phys. Lett. **98**, 012102 (2011).

[54] K. Ueno, S. Nakamura, H. Shimotani, H. T. Yuan, N. Kimura, T. Nojima, H. Aoki, Y. Iwasa, and M. Kawasaki, Nat. Nanotechnol. **6**, 408 (2011).

[55] J. Pu, Y. Yomogida, K.-K. Liu, L.-J. Li, Y. Iwasa, and T. Takenobu, Nano Lett. **12**, 4013 (2012).

[56] W. S. Yun, S. W. Han, S. C. Hong, I. G. Kim, and J. D. Lee, Phys. Rev. B **85**, 033305 (2012).